frontiers | Frontiers in Materials

TYPE Original Research
PUBLISHED 17 June 2025
DOI 10.3389/fmats.2025.1602816

OPEN ACCESS

EDITED BY
Saviour A. Umoren,
King Fahd University of Petroleum and Minerals, Saudi Arabia

REVIEWED BY
Hifsa Khurshid,
King Fahd University of Petroleum and Minerals, Saudi Arabia
Ubong Etim,
The University of Nottingham Ningbo, China

*CORRESPONDENCE
Obaid Afzal,
o.akram@psau.edu.sa

RECEIVED 30 March 2025
ACCEPTED 02 June 2025
PUBLISHED 17 June 2025

CITATION
Altharawi A, Aldakhil T, Alossaimi MA and Afzal O (2025) Harnessing the power of novel ruthenium-MOF for efficient wastewater treatment.
Front. Mater. 12:1602816.
doi: 10.3389/fmats.2025.1602816

Harnessing the power of novel ruthenium-MOF for efficient wastewater treatment

Ali Altharawi, Taibah Aldakhil, Manal A. Alossaimi and Obaid Afzal*

Department of Pharmaceutical Chemistry, College of Pharmacy, Prince Sattam Bin Abdulaziz University, Al-Kharj, Saudi Arabia

A novel metal-organic framework (MOF) was synthesized using 4,4'-(diazene-1,2-diyl)dibenzoic acid and ruthenium (III) chloride via microwave-assisted synthesis. The resulting ruthenium-MOF exhibited a high specific surface area (1856 m^2/g), and the inclusion of ruthenium, known for its biological activity, endowed the structure with potent antimicrobial properties against key wastewater bacterial strains. Furthermore, its abundant hydrogen bonding sites enhanced its adsorption capacity for phenol red, a major waterborne pollutant. The synthesized MOF demonstrated superior antimicrobial activity compared to certain commercial antibiotics. In adsorption experiments, 0.06 g/L of the MOF successfully removed 92% of 0.6 mg/L phenol red at pH 7 within 75 min, highlighting its rapid and efficient pollutant removal capability. These dual functions, antimicrobial and adsorptive, emphasize the potential of this ruthenium-MOF for practical environmental remediation and wastewater treatment applications.

KEYWORDS

ruthenium-based MOF, absorbent, bacterial inhibitor, biological polluta nts, chemical pollutants

1 Introduction

Phenol red is a widely used water-soluble dye that functions primarily as a pH indicator. It exhibits a color transition from yellow to red within the pH range of 6.6–8.0 and turns bright pink at pH values above 8.1 (Steinegger et al., 2020). Due to its sensitivity to pH changes, phenol red finds extensive applications in biomedical research, histology (Benson et al., 2022), environmental monitoring (Idris et al., 2024), culture media (Raffay et al., 2022), pool testing kits (Qin et al., 2023), and cell culture systems (Weiskirchen et al., 2023). Although it is not classified as carcinogenic, concerns regarding its toxicological effects have been raised. Contact with skin may lead to sensitization and irritation (Olusegun and Martincigh, 2021), while eye exposure can result in damage (Kecskeméti et al., 2022). Ingestion is also considered hazardous (DeLoid et al., 2024; An et al., 2025). Given its widespread usage and environmental persistence, phenol red is commonly detected in wastewater and is regarded as a potentially harmful pollutant.

In addition to chemical contaminants such as phenol red, wastewater is frequently burdened with biological pollutants, particularly pathogenic microorganisms. Bacteria *including Salmonella enterica*, *C. jejuni*, *E. coli*, *L. pneumophila*, and *Shigella dysenteriae* are commonly identified in untreated or poorly treated wastewater (Bej et al., 2023; Singh et al., 2024). These pathogens pose serious health threats: *S. enterica* is responsible for typhoid fever (Abro et al., 2024); *Campylobacter jejuni* causes fever and watery diarrhea (Zouganeli et al., 2024); *Escherichia coli* is associated with gastroenteritis (Roy et al., 2024); *Legionella pneumophila* may lead to Pontiac fever (Perez Ortiz et al., 2021); and *S. dysenteriae* results in severe dysentery and intestinal ulceration (Moxley, 2022). Effective strategies are therefore required to remove both chemical and biological pollutants from wastewater to safeguard public and environmental health.

A variety of methods have been investigated for phenol red removal, including chemical treatments (Abu-Nada et al., 2021) and adsorption techniques employing nanomaterials (Ho, 2022; Mousavi et al., 2023). Among advanced adsorbents, metal-organic frameworks (MOFs) have gained considerable attention due to their tunable porosity, high surface area, and diverse chemical functionalities (Song and Qin, 2022).

Some MOFs have demonstrated promising industrial and biomedical applications, including catalysis (Wang et al., 2025) and antibacterial activity (Li et al., 2025). Their antimicrobial properties are often attributed to the presence of metal centers, which disrupt microbial membranes, and to structural features such as porosity and surface area that promote physical entrapment or interaction with pathogens (Borsagli et al., 2019; Li et al., 2021; Arunkumar et al., 2024; Ding et al., 2024; Sharafudheen et al., 2024). High specific surface area in particular enhances contact between the MOF surface and target pollutants, thereby improving both adsorption efficiency and antimicrobial activity (Farasati Far, 2024; Hu et al., 2024; Yao et al., 2024; Zhang et al., 2024).

Ruthenium is a transition metal known for its biological activity and has been incorporated into various MOFs with demonstrated potential for therapeutic and environmental applications (Nakhjiri et al., 2022; Skoczynska et al., 2023). Ruthenium-based compounds have shown anti-inflammatory and antimicrobial properties (Southam et al., 2017; Singh and Barman, 2021; Liu et al., 2022), and their integration into MOF structures can enhance resistance to degradation while preserving or even improving functional performance (Naseer et al., 2022; Rajendran et al., 2024).

In this study, a novel ruthenium-based MOF was synthesized using ruthenium (III) chloride and 4,4'-(diazene-1,2-diyl)dibenzoic acid. Owing to its large specific surface area and presence of biologically active sites, the material was evaluated for its capacity to adsorb phenol red and inhibit bacterial pathogens commonly found in wastewater. The results demonstrated that the synthesized ruthenium-MOF exhibited high efficacy in removing both chemical and biological contaminants. The antimicrobial activity of ruthenium, coupled with the MOF's porosity and extensive surface area, contributes to its strong potential for dual-function wastewater treatment. This underscores the novelty and practical relevance of our findings in addressing complex pollution challenges.

2 Materials and methods

2.1 Material and devises

Ruthenium (III) chloride (99.95%, Otto Chemie Pvt. Ltd.) and 4,4'-(diazene-1,2-diyl)dibenzoic acid (95%, Ambeed) were used as precursors for the synthesis of the ruthenium-MOF. Mueller Hinton Agar and Mueller Hinton Broth (HiMedia) were utilized for antimicrobial studies, and bacterial strains were obtained from the American Type Culture Collection (ATCC). Phenol red (analytical grade), sodium hydroxide (99.95%, Merck), and hydrochloric acid (37%, Merck) were used in the phenol red adsorption studies.

A BP211 laboratory-grade microwave reactor was employed for MOF synthesis, while an LMSP-UV1000B UV-Visible spectrophotometer was used to assess pollutant adsorption and antimicrobial efficacy.

2.2 Synthesis of ruthenium-MOF

To synthesize the ruthenium-MOF, 1 mmol of ruthenium (III) chloride and 2 mmol of 4,4'-(diazene-1,2-diyl)dibenzoic acid were dissolved in 25 mL of deionized water and stirred at 500 rpm at room temperature until a homogeneous solution was obtained. The mixture was then exposed to microwave irradiation. The temperature was gradually increased from 25°C to 180°C at a rate of 10°C/min and maintained at 180°C for 20 min under continuous irradiation at 320 W. After cooling for 30 min, the resulting precipitate was separated via nanofiltration, washed three times with a 1:1 mixture of deionized water and ethanol, and dried under vacuum at 100°C for 4 h (Al-dolaimy et al., 2023; Ahmad et al., 2024)

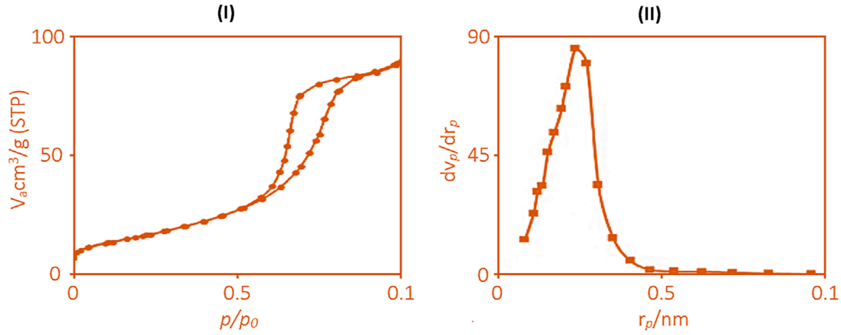

FIGURE 1
Nitrogen adsorption and desorption curve of synthesized ruthenium-MOF [(I): BET, b (II): BJH].

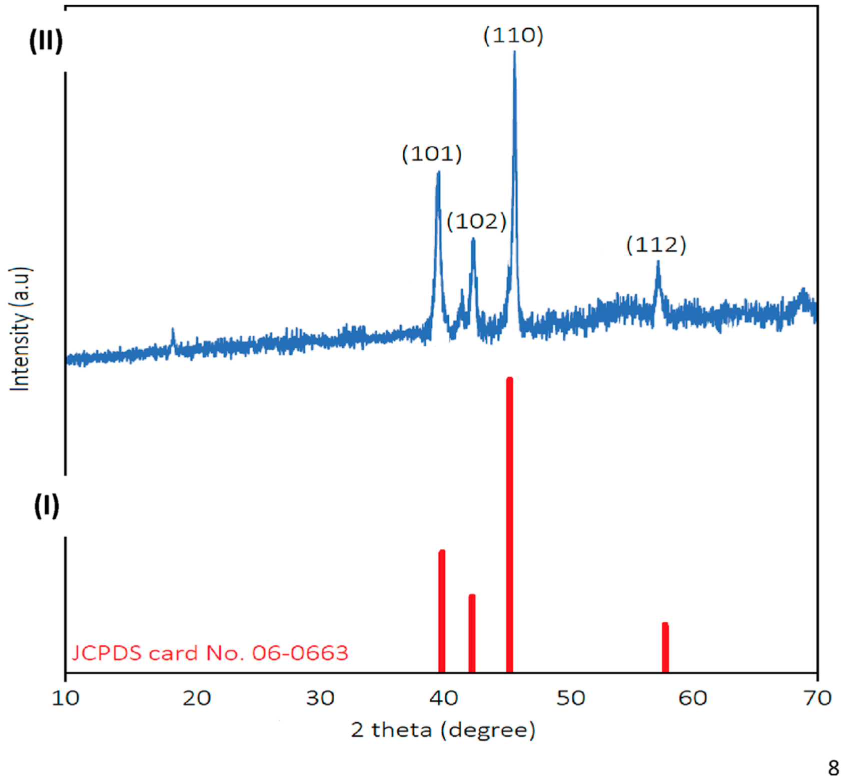

FIGURE 2
XRD of synthesized ruthenium-MOF (I): Reported JCPDS No 06-0663 for ruthenium; (II): Synthesized ruthenium-MOF).

TABLE 1 N_2 adsorption-desorption of ruthenium-MOF.

Brunauer–Emmett–Teller (m^3/g)	Barett-Joyner-Halenda (cm^3/g)	Mean pore diameter (nm)
1856	0.46	1.37

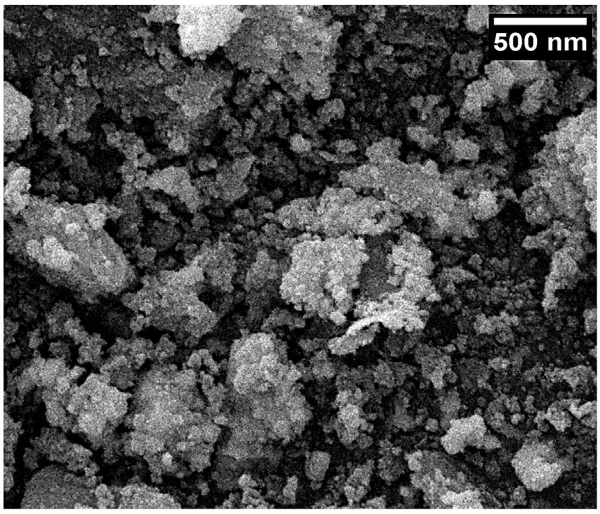

FIGURE 3
SEM image of synthesized ruthenium-MOF.

TABLE 2 EA result of ruthenium-MOF.

C (%)	H (%)	N (%)	O (%)
52.83	3.46	8.21	19.08

2.3 Characterization

To confirm the structure and properties of the synthesized ruthenium-MOF, the following characterization techniques were used:

Nitrogen adsorption/desorption analysis: Conducted at 77 K with relative pressures from 0.01 to 0.99 using the ASAP 2020 instrument to determine BET surface area and pore size distribution via BJH or DFT models.

X-ray diffraction (XRD): Performed using Cu Kα radiation at 40 kV/30 mA over a 2θ range of 10°–70°, with a step size of 0.02° and scan speed of 1 s/step (Drawell DW-XRD-27Mini Desktop).

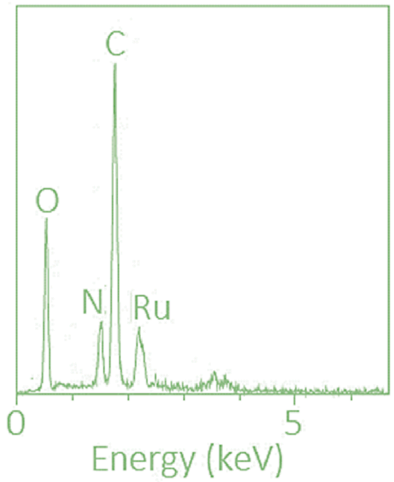

FIGURE 4
EDAX of synthesized ruthenium-MOF.

Scanning electron microscopy (SEM) and energy-dispersive X-ray spectroscopy (EDAX): Conducted using a TESCAN VEGA 3 at 15 kV with a working distance of 10 mm in high vacuum mode.

Elemental analysis (CHNO): Carried out using a FlashSmart Elemental Analyzer by combustion in excess oxygen at 1100°C.

Fourier-transform infrared spectroscopy (FT-IR): Acquired using the KBr pellet method on a DW-FTIR-530A Drawell spectrometer.

Thermogravimetric analysis (TGA): Conducted from 25°C to 600°C at a heating rate of 10°C/min using a GA BXT-TGA-1250.

2.4 Wastewater treatment

2.4.1 Inhibition of biological agents

The antimicrobial efficacy of the synthesized ruthenium-MOF was assessed using a range of concentrations (1–1024 µg/mL) against bacterial suspensions (1×10^5 CFU/mL) of selected wastewater pathogens. The methods and standards established by the Clinical and Laboratory Standards Institute (CLSI) were followed in accordance with previous studies (Moghaddam-Manesh et al., 2020; Hsu et al., 2024). The tests performed included:

Minimum Inhibitory Concentration (MIC): A mixture of 100 µL of ruthenium-MOF solution (various concentrations), 100 µL of Mueller Hinton Broth, and 10 µL of bacterial suspension was incubated at 37°C for 48 h. The MIC was defined as the lowest concentration that completely inhibited visible bacterial growth (Moghaddam-Manesh et al., 2020; Hsu et al., 2024).

Minimum Bactericidal Concentration (MBC): Aliquots from the MIC test and subsequent dilutions were plated on Mueller Hinton Agar and incubated at 37°C for 72 h. The MBC was recorded as the lowest concentration at which no bacterial colonies were observed (Moghaddam-Manesh et al., 2020; Hsu et al., 2024).

Inhibition Zone Diameter (IZD): The disk diffusion method was employed using sterile paper disks impregnated with 10 µL of ruthenium-MOF at MIC concentrations. The disks were placed on inoculated agar plates and incubated at 37°C for 48 h. The diameter of the inhibition zone was measured using calipers (Moghaddam-Manesh et al., 2020; Hsu et al., 2024).

2.4.2 Adsorption of chemical agents

Phenol red adsorption experiments were conducted using different initial dye concentrations, MOF dosages, pH levels (4-10), temperatures (25°C–60°C), and contact times (25–200 min). In each test, ruthenium-MOF was added to 25 mL of phenol red solution, and the mixture was agitated at 140 rpm. After the desired reaction time, the suspension was centrifuged at 6000 rpm for 10 min, and the absorbance of the supernatant was measured at 430 nm using a UV-Vis spectrophotometer. The removal efficiency (Re, %) was calculated using the Equation 1 (Aljubiri et al., 2024; Moghaddam-Manesh et al., 2024):

$$Re\,(\%) = \left(\frac{C0 - Ce}{C0}\right) \times 100 \tag{1}$$

The initial concentration of phenol red (mg/L) = C_0

The equilibrium concentration of phenol red (mg/L) = C_e

Equation 1. Phenol red adsorption percentage using ruthenium-MOF.

3 Result and discussion

3.1 Synthesis and characterization

Microwave-assisted synthesis has emerged as a rapid and efficient method for producing metal-organic frameworks (MOFs) with desirable physicochemical properties. This technique has been reported to yield MOFs with high crystallinity, nanoscale particle size, and large specific surface area (Głowniak et al., 2021; Annamalai et al., 2022). In this study, a ruthenium-based MOF was successfully synthesized using ruthenium (III) chloride and 4,4'-(diazene-1,2-diyl)dibenzoic acid under controlled microwave conditions, following previously optimized protocols (Al-dolaimy et al., 2023; Ahmad et al., 2024).

Nitrogen adsorption/desorption analysis revealed that the synthesized MOF exhibits a remarkably high specific surface area of 1856 m^2/g, as illustrated in Figure 1. The isotherms corresponded to a type IV profile, characteristic of mesoporous materials (Calzaferri et al., 2022; Hu et al., 2023; Peng et al., 2024).

The surface area and pore characteristics, including BET surface area, Barrett–Joyner–Halenda (BJH) pore volume, and mean pore diameter (MPD), are summarized in Table 1.

X-ray diffraction (XRD) analysis confirmed the crystalline nature of the synthesized MOF (Figure 2). Distinct diffraction peaks were observed at 2θ values of 39.9°, 42.1°, 44.8°, and 58.3°, corresponding to the (101), (102), (110), and (112) planes, respectively, as referenced by JCPDS card No. 06-0663 (Tee et al., 2015; Pang et al., 2021; Wang et al., 2023). The average crystallite size, calculated using the Scherrer equation, was approximately 92 nm (Holzwarth and Gibson, 2011; Nasiri et al., 2023).

Scanning electron microscopy (SEM) revealed uniform morphology with particle sizes averaging 85 nm and no observable agglomeration (Figure 3).

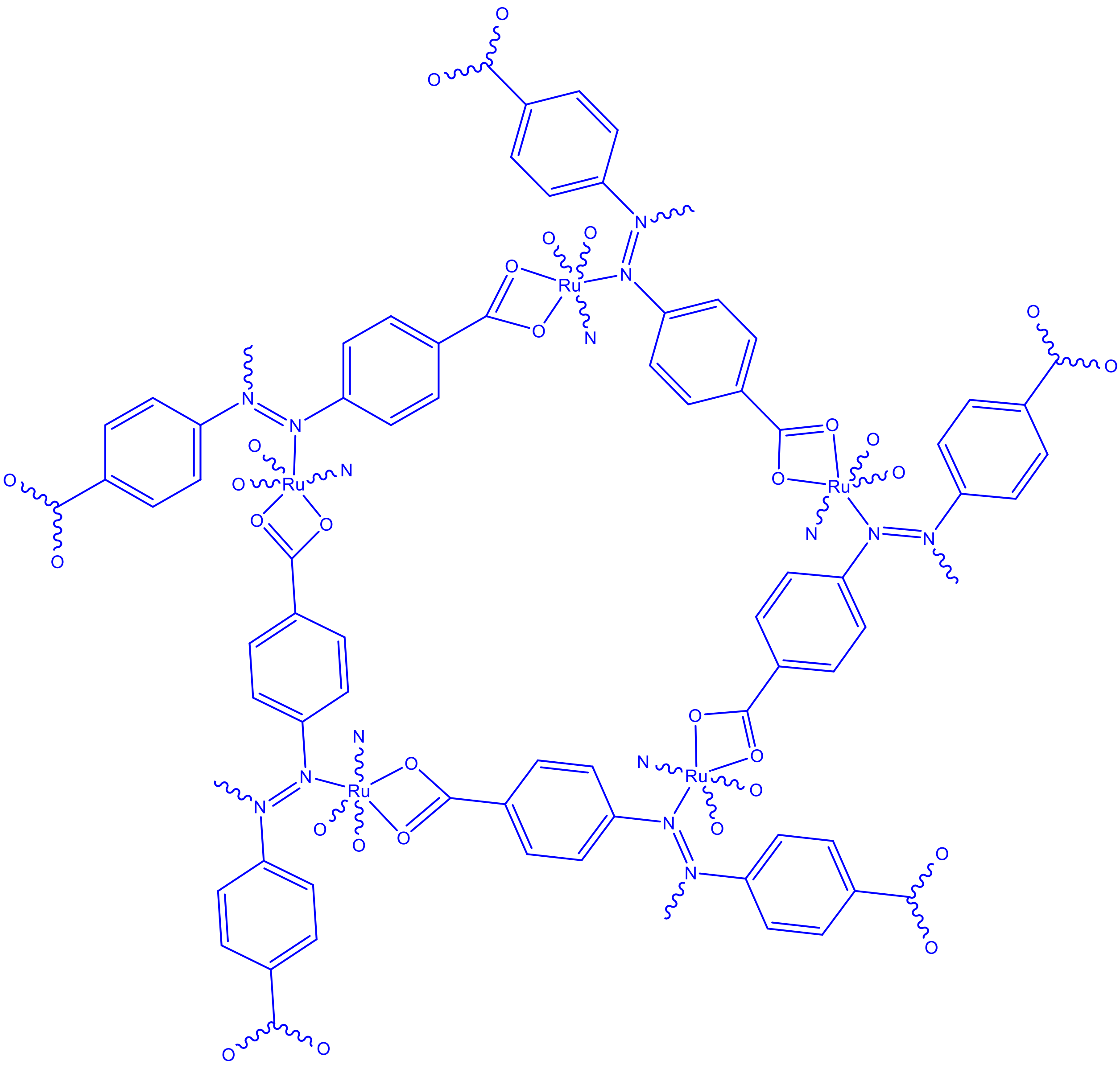

FIGURE 5
Structure of synthesized ruthenium-MOF.

These findings confirm that the adopted synthesis method is effective for producing a highly crystalline and nanoscale MOF with significant surface area and porosity.

Elemental analysis and energy-dispersive X-ray spectroscopy (EDAX) were employed to confirm the presence of ruthenium and other constituent elements. The results are presented in Table 2; Figure 4.

The proposed molecular structure of the ruthenium-MOF, shown in Figure 5, is consistent with the XRD and elemental analysis data.

Fourier-transform infrared (FT-IR) spectroscopy further verified the structural integrity of the MOF. The spectrum of the synthesized product (Figures 6–II) demonstrated characteristic absorption bands: Ru–N and Ru–O bonds in the 400–600 cm^{-1} region (Feng et al., 2022; Jin et al., 2022; Akl et al., 2023), C-H at 3025 cm^{-1}, C=O at 1680 cm^{-1}, N=N at 1565 cm^{-1}, C=C at 1460 cm^{-1}, N-C at 1100 cm^{-1}, and C-O at 1025 cm^{-1}. The broad O–H peak at 3250 cm^{-1}, present in the free ligand, was absent in the MOF spectrum, suggesting successful coordination of the ligand through its oxygen atoms.

The FT-IR spectrum of the ruthenium-MOF, as shown in Figures 6–II, confirms the presence of the ligand in the structure, as all ligand peaks are observed. Additionally, the broad oxygen-hydrogen peak (3250 cm^{-1}), which is absent in the FTIR spectrum of the ruthenium-MOF, indicates the binding of the 4,4'-(diazene-1,2-diyl)dibenzoic acid to the ruthenium through the oxygen side. Therefore, oxygen-ruthenium and nitrogen-ruthenium bonds, observed in previous studies in the 400 cm^{-1} - 600 cm^{-1} (Feng et al., 2022; Jin et al., 2022; Akl et al., 2023), and two peaks have been

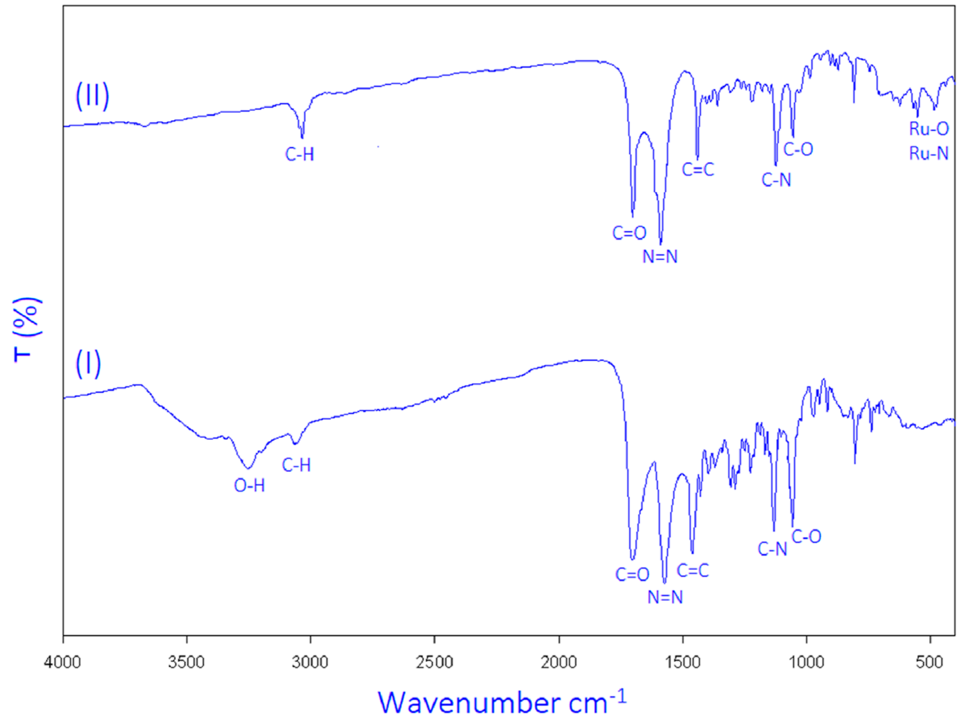

FIGURE 6
FT-IR spectrum of 4,4'-(diazene-1,2-diyl)dibenzoic acid (I) and synthesized ruthenium-MOF (II).

observed in this area, so Ru-N and Ru-O are sites of ruthenium complexation with the 4,4'-(diazene-1,2-diyl)dibenzoic acid, as seen in the FTIR spectrum of the ruthenium-MOF.

Thermogravimetric analysis (TGA) demonstrated the thermal stability of the ruthenium-MOF. The material remained stable up to approximately 350°C, with two major weight loss events observed around 350°C and 520°C. These correspond to the decomposition of the organic ligand and subsequent breakdown of the MOF network.

3.2 Wastewater treatment results

Given the characterization of the newly synthesized ruthenium-MOF, which had a high specific surface area and high porosity, and the antimicrobial nature of ruthenium, the antimicrobial properties and phenol adsorption were investigated and discussed below.

3.2.1 Results of inhibition of biological agents

As mentioned in the introduction, *Salmonella enterica (ATCC 35664), Campylobacter jejuni (ATCC 700819), Escherichia coli (ATCC 25922), Legionella pneumophila (ATCC 33152), and Shigella dysenteriae (ATCC 13313)* can be identified as the most important pathogenic agents present in wastewater. The investigation of the inhibition properties of these biological agents by the ruthenium-MOF was conducted using MIC and MBC, as well as measuring the IZD. The findings of these studies are presented in Table 3.

The results from the table indicate that the ruthenium-MOF was able to inhibit all the studied strains, with MIC values of 32 μg/mL *Salmonella enterica*, 16 μg/mL *Campylobacter jejuni*, 1 μg/mL against *Escherichia coli*, 32 μg/mL against *Legionella pneumophila*, and 128 μg/mL against *Shigella dysenteriae*.

As mentioned, high specific surface area of synthesized ruthenium-MOF and more excellent contact with the studied bacterial agents, along with the presence of a ruthenium compound with strong antibacterial properties and a ligand known to possess several antibacterial properties (Southam et al., 2017; Singh and Barman, 2021; Pourmadadi et al., 2023; Tan et al., 2023), can be considered factors contributing to the effective inhibition of the studied strains. Additionally, *C. jejuni*, *L. pneumophila*, and *S. dysenteriae* were resistant to cefazolin, and *S. dysenteriae* were resistant to azithromycin, a well-known antibiotic on the market, indicating that the compound synthesized in this study has superior antibacterial properties compared to cefazolin.

Each experiment was independently conducted three times to ensure reproducibility. The MIC and MBC values remained stable across replicates, while the inhibition zone diameters (IZD) are summarized as mean values with corresponding standard deviations (SD). Statistical significance was assessed using p-values to examine the influence of compound concentration on antibacterial activity. The findings suggest a strong concentration-dependent effect on MIC, MBC, and IZD parameters, particularly for the tested Ruthenium-MOF and Azithromycin compounds.

3.2.2 Results of adsorption of chemical agents

The ruthenium-MOF demonstrated excellent adsorption performance for phenol red, attributable to its high surface area, porosity, and abundance of hydrogen bonding sites (Wu et al., 2020; Lau et al., 2022; Zhou et al., 2024). Phenol red exists in two

TABLE 3 Antimicrobial results.

Compounds	Parameters		Strains				
			Salmonella enterica	*Campylobacter jejuni*	*Escherichia coli*	*Legionella pneumophila*	*Shigella dysenteriae*
Ruthenium-MOF	MIC (mg/mL)	Amount	32	16	1	32	128
		p-value	0.01	0.03	0.03	0.00	0.002
	MBC (mg/mL)	Amount	64	32	2	64	256
		p-value	0.00	0.01	0.04	0.00	0.02
	IZD (mm)	Amount	12.67 ± 0.9	15.29 ± 1.2	20.77 ± 0.9	13.46 ± 0.9	12.92 ± 0.9
		p-value	0.01	0.01	0.02	0.00	0.03
Cefazolin	MIC (mg/mL)	Amount	32	Ineffectiveness	2	Ineffectiveness	Ineffectiveness
		p-value	0.04	Ineffectiveness	0.00	Ineffectiveness	Ineffectiveness
	MBC (mg/mL)	Amount	64	Ineffectiveness	4	Ineffectiveness	Ineffectiveness
		p-value	0.01	Ineffectiveness	0.02	Ineffectiveness	Ineffectiveness
	IZD (mm)	Amount	15.31	Ineffectiveness	21.67	Ineffectiveness	Ineffectiveness
		p-value	0.03	Ineffectiveness		Ineffectiveness	Ineffectiveness
Azithromycin	MIC (μg/mL)	Amount	8	8	1	16	Ineffectiveness
		p-value	0.00	0.04	0.01	0.00	Ineffectiveness
	MBC (mg/mL)	Amount	16	8	2	32	Ineffectiveness
		p-value	0.02	0.03	0.01	0.04	Ineffectiveness
	IZD (mm)	Amount	19.08	18.69	22.81	17.54	Ineffectiveness
		p-value	0.01	0.00	0.00	0.03	Ineffectiveness

tautomeric forms depending on pH: one in acidic conditions (7-I) and another in alkaline conditions (7-II). The synthesized MOF was able to adsorb phenol red in both environments through hydrogen bonding and electrostatic interactions, as depicted in Figures 7–III.

To evaluate the adsorption performance, several experimental parameters were optimized, including initial dye concentration, adsorbent dose, pH, temperature, and contact time.

3.2.2.1 Phenol red concentration effect

Phenol red concentrations ranging from 100 to 1000 mg/L were tested using 0.01 g of ruthenium-MOF under fixed conditions (pH 7, 25°C, 50 min). As shown in Figures 8–I, the adsorption efficiency decreased with increasing dye concentration. This inverse relationship is attributed to the limited number of active hydrogen bonding sites, which become saturated at higher dye concentrations (Zhang et al., 2021).

3.2.2.2 Amount of adsorbent effect

To identify the optimal adsorbent dosage, various concentrations of ruthenium-MOF (0.01–0.10 g/L) were tested. The results (Figures 8–II) indicate that adsorption increased with increasing adsorbent amount, reaching a plateau at 0.06 g/L. Beyond this point, additional adsorbent did not significantly improve removal efficiency, likely due to particle agglomeration and site carbonization (Poon et al., 2022). Therefore, 0.06 g/L was used in subsequent experiments.

3.2.2.3 pH effect

Phenol red adsorption was evaluated across a pH range of 4–10, maintaining constant adsorbent dose, temperature, and contact time. Maximum adsorption occurred at pH 8 (Figures 8–III). At this pH, the anionic form of phenol red interacts more effectively with electron-rich oxygen and nitrogen atoms in the MOF structure. Conversely, extreme acidic and alkaline conditions were detrimental to adsorption, likely due to hydrolysis or protonation effects (Siddique et al., 2024; Pessoa and Correia, 2021; Yesil et al., 2021). Nevertheless, since the difference between pH 7 and pH 8 was minimal, further tests were conducted at neutral pH.

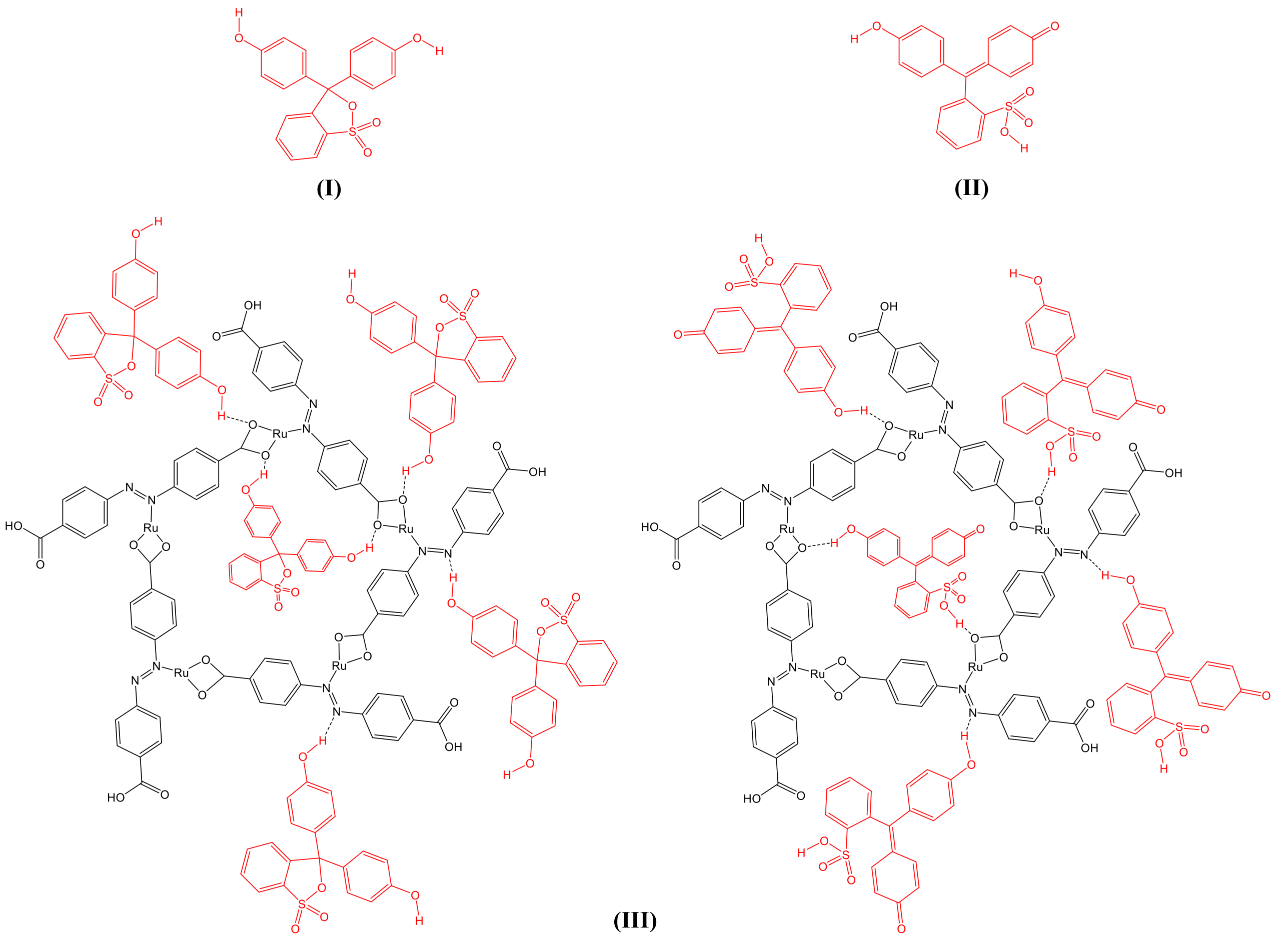

FIGURE 7
Structure of phenol red in acidic (I) and alkaline (II) environments and its adsorption by synthesized ruthenium-MOF (III).

3.2.2.4 Temperature effect

Temperature variation (25°C–60°C) showed a positive correlation with adsorption performance (Figures 8–IV). Higher temperatures enhanced molecular motion and diffusion rates, resulting in increased adsorption of phenol red (Qiu et al., 2022).

3.2.2.5 Time effect

Adsorption were evaluated over contact times ranging from 30 to 120 min. Maximum adsorption occurred at 75 min, after which equilibrium was reached (Figures 8–V). The saturation of active adsorption sites explains the observed plateau beyond this time point.

The excellent adsorption performance is largely attributed to the high surface area and mesoporosity of the MOF structure, which provide abundant access to active binding sites (Dendy et al., 2025). Under optimal conditions (0.06 g/L MOF, 0.6 mg/L phenol red, pH 7, 25°C, 75 min), the ruthenium-MOF achieved 92% removal efficiency (23 mg/g), outperforming several previously reported MOFs (Table 4).

Compared to the uranyl-curcumin-MOF (Khandan et al., 2018), which only removed 0.11 mg/L, the ruthenium-MOF performed significantly better. While some other MOFs (e.g., Cu-BTC) showed higher absolute adsorption capacities, they were tested against different dyes, often at higher concentrations and under different conditions. The advantage of ruthenium-MOF lies in its fast kinetics, high surface area, and ability to work efficiently at neutral pH, making it highly practical for real wastewater treatment.

3.2.3 Reusability

After the adsorption process, the synthesized ruthenium-MOF was washed three times with water and ethanol and it was placed in an oven at 100°C for 4 h under vacuum conditions. It's TGA (Figures 9–I), FT-IR (Figures 9–II), and XRD (Figures 9–II) was prepared and no significant change was observed compared to before use. Only in the TGA curve was a weight loss observed near 100°C, which can be attributed to the evaporation of water absorbed on the surface or pores of the MOF, which occurred during the absorption or washing process. Then, the adsorption process was re-evaluated under obtained optimal conditions. The results showed that under obtained optimal conditions, including phenol red concentrations (0.6 mg/L), ruthenium-MOF concentrations (0.06 g/L), pH (7), temperature (25°C), and time (75 min), the percentage adsorption did not change significantly up to three times (Figures 9–IV).

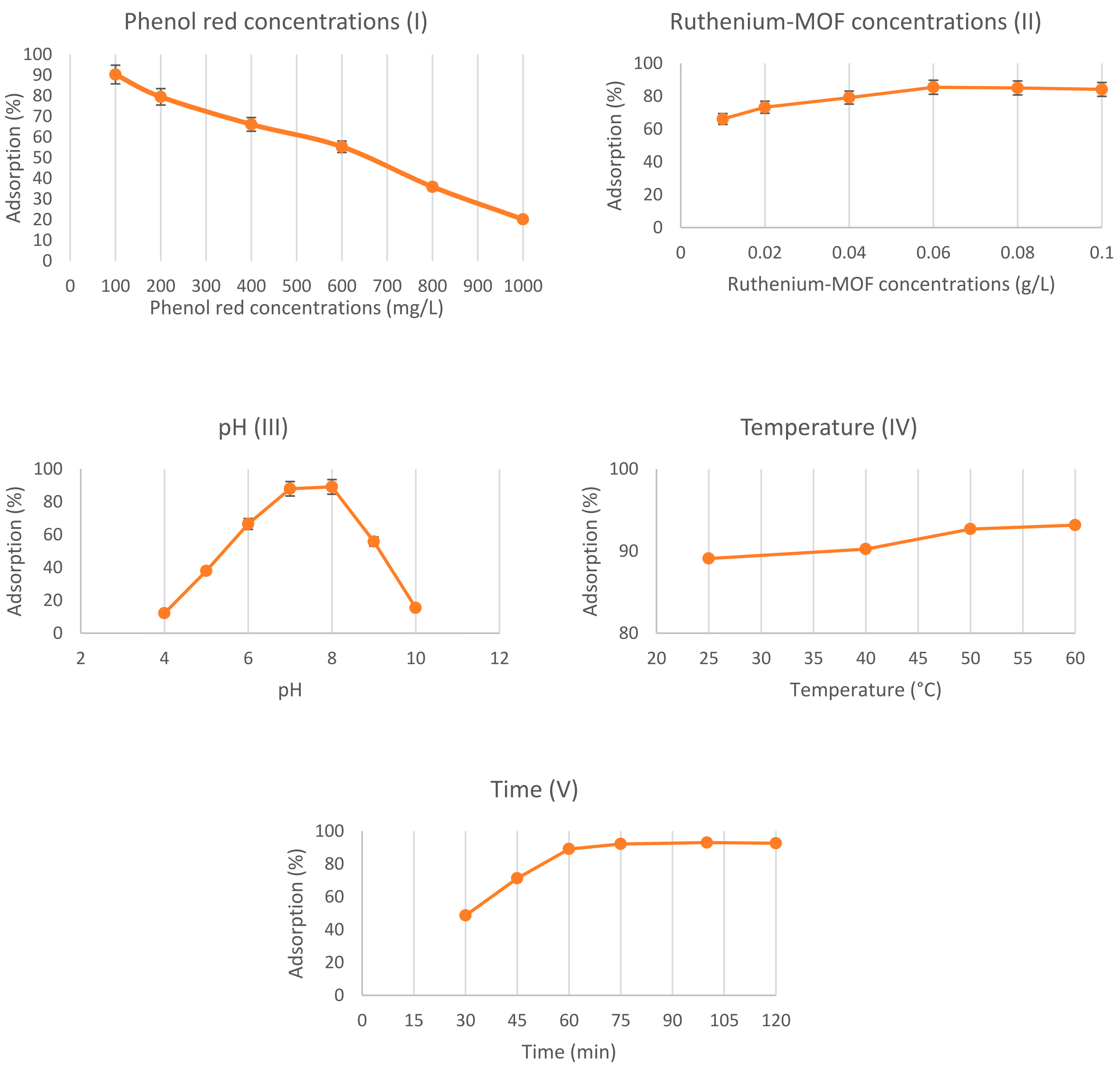

FIGURE 8
Phenol red adsorption study results using synthesized ruthenium-MOF (I: Phenol red concentrations, II: Ruthenium-MOF concentrations, III: pH, IV: Temperature, V: Time).

TABLE 4 **Comparison dye adsorption of ruthenium-MOF with other MOFs.**

MOF type	Target dye	Optimal conditions	Adsorption capacity	Reference
Ruthenium-MOF (This work)	Phenol red	pH 7, 0.06 g/L, 75 min, 25°C	~23 mg/g (92% of 0.6 mg/L)	Current document
Uranyl-Curcumin-MOF	Phenol red	pH 8	0.11 mg/L	Khandan et al. (2018)
MIL-101(Fe)	Congo red	pH 6, 60 min	~180 mg/g	Siddique et al. (2024)
ZIF-8	Methyl orange	pH 4, 120 min	~90 mg/g	Ho (2022)
Cu-BTC	Rhodamine B	pH 7, 60 min	~250 mg/g	Mousavi et al. (2023)
MOF@Chitosan Composite	Phenol red	pH 7, 40 min	~45 mg/g	Lau et al. (2022)

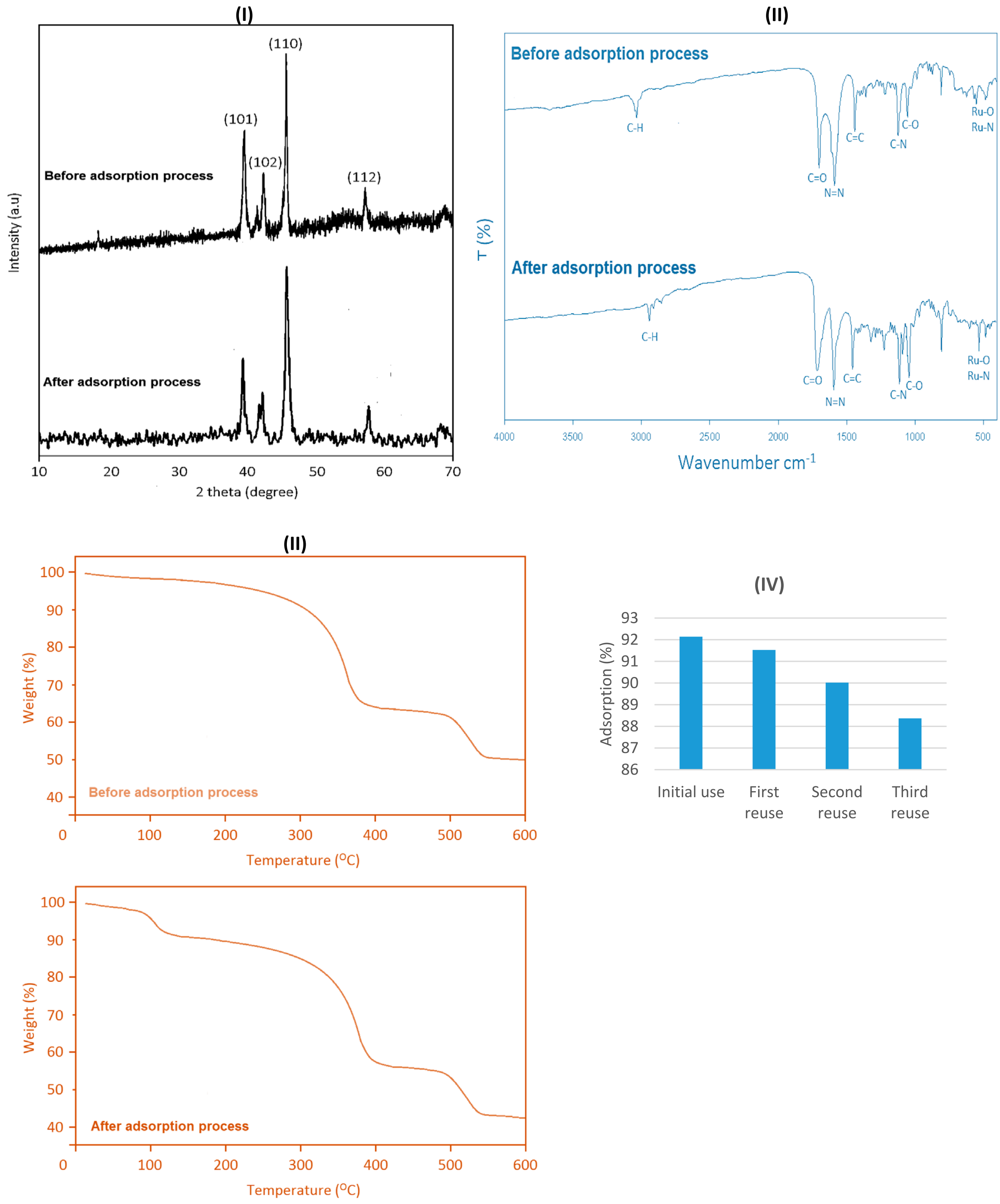

FIGURE 9
XRD (I), FT-IR (II) and TGA (III) of ruthenium-MOF after the adsorption process, and its reusability in phenol red adsorption (IV).

3.2.4 Kinetic modeling in phenol red adsorption using ruthenium-MOF

To investigate the adsorption mechanism and rate-controlling steps, kinetic studies were conducted using pseudo-first-order and pseudo-second-order models. These models provide insight into the nature of the interaction between phenol red molecules and the active sites of the ruthenium-MOF.

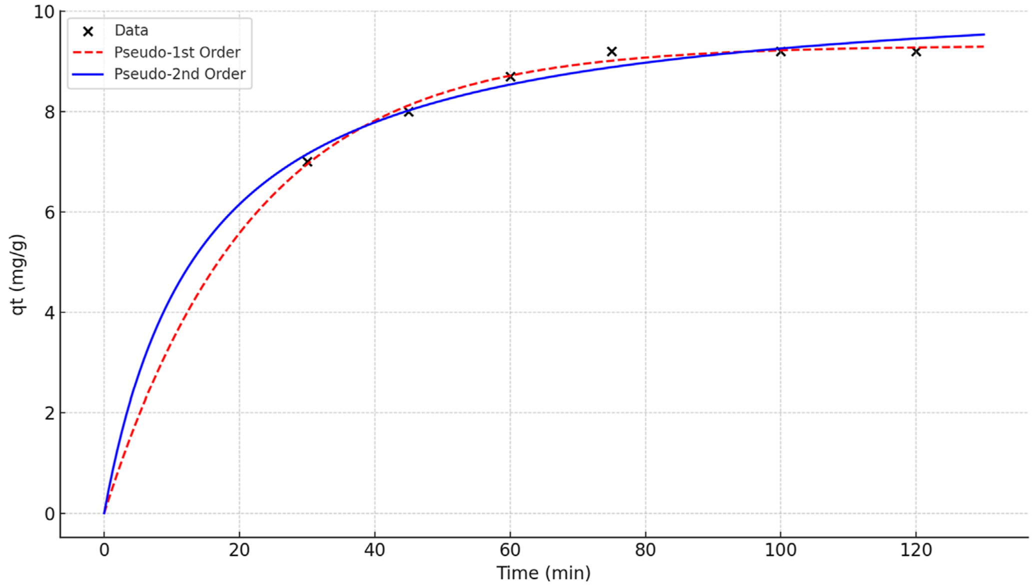

FIGURE 10
Kinetic modeling of phenol red adsorption using ruthenium-MOF.

TABLE 5 Kinetic model parameters phenol red adsorption using ruthenium-MOF.

Kinetic model	Parameter	Value	Description
Pseudo-first-order	k_1 (min^{-1})	0.0457	Rate constant
Pseudo-first-order	q_e (mg/g)	9.32	Equilibrium adsorption capacity
Pseudo-second-order	k_2 ($g \cdot mg^{-1} \cdot min^{-1}$)	0.00655	Rate constant
Pseudo-second-order	q_e (mg/g)	10.59	Equilibrium adsorption capacity

3.2.4.1 Pseudo-first-order

The pseudo-first-order equation is as follows (Equation 2):

$$\ln(qe - qt) = \ln qt - k_1 t \tag{2}$$

$k_1 = 0.0457\ min^{-1}$
$q_e = 9.32$ mg/g.

Equation 2. Pseudo-first-order in phenol red adsorption using ruthenium-MOF.

Suitable when the adsorption rate depends on available vacant sites.

3.2.4.2 Pseudo-second-order

The pseudo-second-order is as follows (Equation 3):

$$\frac{t}{qt} = \frac{1}{k_2 qe^2} + \frac{t}{qe} \tag{3}$$

$k_2 = 0.00655$ g/mg.min.
$q_e = 10.59$ mg/g.

Equation 3. Pseudo-second-order in phenol red adsorption using ruthenium-MOF.

Assumes chemisorption as the rate-limiting step.

Based on the results in Figure 10; Table 5, the pseudo-second-order model fits the data better and predicts a higher adsorption capacity, which is consistent with the assumption of chem-adsorption. Also, the saturation of the adsorbent surface at ~75 min is also consistent with the behavior of the second model.

3.2.5 Isotherm modeling in phenol red adsorption using ruthenium-MOF

To better understand the adsorption behavior and surface interactions, isotherm models were applied. Both Langmuir and Freundlich models were evaluated using experimental equilibrium data.

3.2.5.1 Langmuir isotherm

The Langmuir isotherm equation is as follows (Equation 4):

$$qe = \frac{q_{\max} K_L Ce}{1 + K_L Ce} \tag{4}$$

$q_{\max} = 1000$ mg/g.
$K_L = 0.0314$ L/mg.

Equation 4. Langmuir isotherm in phenol red adsorption using ruthenium-MOF.

3.2.5.2 Freundlich isotherm

The Freundlich isotherm equation is as follows (Equation 5):

$$qe = K_F Ce^{1/n} \tag{5}$$

KF = 164.79.
$n = 3.33$.

Equation 5. Freundlich isotherm in phenol red adsorption using ruthenium-MOF.

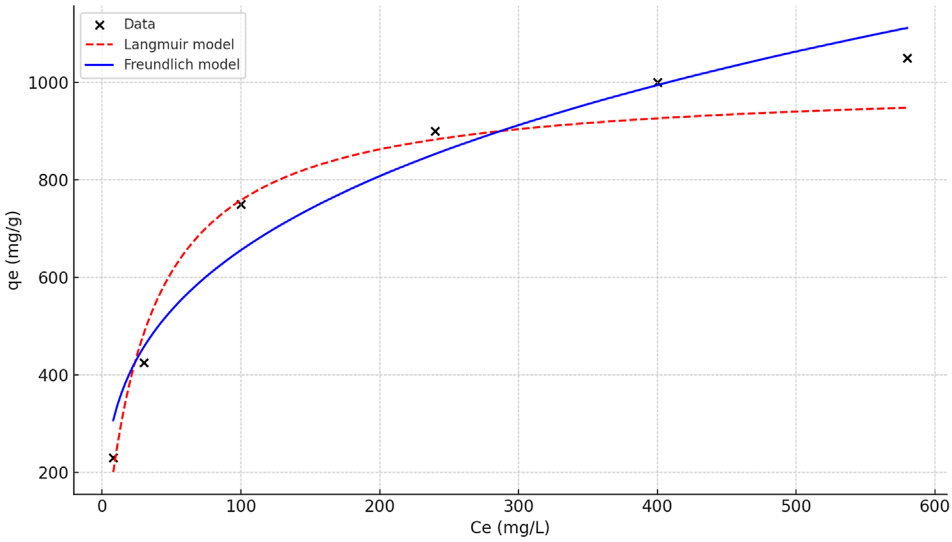

FIGURE 11
Isotherm modeling of phenol red adsorption using ruthenium-MOF.

TABLE 6 Isotherm model parameters phenol red adsorption using ruthenium-MOF.

Isotherm model	Parameter	Value	Description
Langmuir	q_{max} (mg/g)	1000	Maximum adsorption capacity (approximate)
Langmuir	K_L (L/mg)	0.0314	Langmuir constant
Freundlich	K_F [(mg/g)(L/mg)$^{1/n}$]	164.79	Adsorption capacity constant
Freundlich	n	3.33	Adsorption intensity (n > 1 indicates favorable adsorption)

Based on the results in Figure 11; Table 6, the Freundlich model better represents the system and supports a heterogeneous multilayer adsorption process.

4 Conclusion

In light of the human need for clean water and the challenges posed by population growth, climate change, and limited freshwater resources, this study focuses on the synthesis of a new metal-organic framework (ruthenium-MOF) and its application in treating biological pollutants, specifically the inhibition of bacterial strains *Salmonella enterica*, *Campylobacter jejuni*, *Escherichia coli*, *Legionella pneumophila*, and *Shigella dysenteriae*, which are among the most significant pathogens found in wastewater. Additionally, this MOF was designed to remove chemical pollutants such as phenol red, a compound associated with various diseases and skin irritations. The synthesized MOF incorporates ruthenium and 4,4'-(diazene-1,2-diyl)dibenzoic acid as structural components. The biological properties of these compounds, along with the high specific surface area of the ruthenium-MOF, contribute to its unique ability to eliminate both biological and chemical contaminants from wastewater. In biological tests, the MOF showed higher inhibition rates for certain bacterial strains compared to cefazolin and azithromycin. Regarding chemical pollutant removal, the MOF achieved 92% removal of 0.6 mg/L phenol red using 0.06 g/L of the adsorbent at neutral pH and 75 min. Based on kinetic and isotherm studies, the pseudo-second-order model best described the adsorption process, and the Freundlich model best fit the isotherm data. The synthesized ruthenium-MOF demonstrates great potential as an efficient material for wastewater treatment. Further studies are recommended to evaluate its effectiveness against other biological and chemical pollutants.

Data availability statement

The authors confirm that the data supporting the findings of this study are available within the article.

Author contributions

AA: Writing – original draft. TA: Writing – original draft. MAA: Writing – review and editing. OA: Writing – review and editing.

Funding

The author(s) declare that financial support was received for the research and/or publication of this article. This study is supported via funding from Prince Sattam Bin Abdulaziz University project number (PSAU/2025/R/1446).

Conflict of interest

The authors declare that the research was conducted in the absence of any commercial or financial relationships that could be construed as a potential conflict of interest.

Generative AI statement

The author(s) declare that no Generative AI was used in the creation of this manuscript.

Publisher's note

References

Abro, U. A., Bano, S., Tunio, S. A., and Abassi, S. M. (2024). Antibiotic resistance trends in high-risk lineages of *Salmonella enterica* serovar Typhi: a study spanning pre to post COVID-19 pandemic. *Infect. Genet. Evol.* 123, 105632. doi:10.1016/j.meegid.2024.105632

Abu-Nada, A., Abdala, A., and Mckay, G. (2021). Removal of phenols and dyes from aqueous solutions using graphene and graphene composite adsorption: a review. *J. Environ. Chem. Eng.* 9, 105858. doi:10.1016/j.jece.2021.105858

Ahmad, I., Bishoyi, A. K., Altalbawy, F., Menon, S. V., Chahar, M., Tawfiq, M. M., et al. (2024). Synthesis, identification and introduction of novel Cu/Zn-bmof as a bioactive Bi-metal organic framework. *J. Inorg. Organomet. Polym. Mater.* 35, 3530–3544. doi:10.1007/s10904-024-03474-w

Akl, H. N., Salah, D., Abdel-Samad, H. S., Aziz, A. a.A., and Abdel-Shafi, A. A. (2023). Fractional dependence of the free energy of activation on the driving force of charge transfer in the quenching of the excited states of substituted phenanthroline homoleptic ruthenium (ii) complexes in aqueous medium. *RSC Adv.* 13, 13314–13323. doi:10.1039/d3ra01280h

Al-Dolaimy, F., Altimari, U. S., Abdulwahid, A. S., Mohammed, Z. I., Hameed, S. M., Dawood, A. H., et al. (2023). Hydrogel assisted synthesis of polymeric materials based on chitosan, oxidized pectin, and tantalum MOF nanostructures as potent antibiotic agents against common pathogenic strains between humans and aquatic. *J. Inorg. Organomet. Polym. Mater.* 34, 874–884. doi:10.1007/s10904-023-02863-x

Aljubiri, S. M., Younes, A. A., Alosaimi, E. H., Abdel-Daiem, M. M., Abdel-Salam, E. T., and El-Shwiniy, W. H. (2024). Efficient removal of phenol red dye from polluted water using sustainable low-cost sewage sludge activated carbon: adsorption and reusability studies. *Molecules* 29, 5865. doi:10.3390/molecules29245865

An, X., Abdellah, Y. a.Y., Wang, L., Elsheikh, E. A., Wang, Y., Yang, J., et al. (2025). NaCl as an excellent trigger-induced biodiesel production and phenol-containing wastewater treatment in a novel salt-tolerant microalgae Ankistrodesmus sp. ACC. *Bioresour. Technol.* 429, 132515. doi:10.1016/j.biortech.2025.132515

Annamalai, J., Murugan, P., Ganapathy, D., Nallaswamy, D., Atchudan, R., Arya, S., et al. (2022). Synthesis of various dimensional metal organic frameworks (MOFs) and their hybrid composites for emerging applications–a review. *Chemosphere* 298, 134184. doi:10.1016/j.chemosphere.2022.134184

Arunkumar, T., Castelino, E., Lakshmi, T., Mulky, L., Selvanathan, S. P., and Tahir, M. (2024). Metal–organic frameworks in antibacterial disinfection: a review. *ChemBioEng Rev.* 11, e202400006. doi:10.1002/cben.202400006

Bej, S., Swain, S., Bishoyi, A. K., Mandhata, C. P., Sahoo, C. R., and Padhy, R. N. (2023). Wastewater-associated infections: a public health concern. *Water, Air, and Soil Pollut.* 234, 444. doi:10.1007/s11270-023-06431-4

Benson, M. D., Berk, J. L., Dispenzieri, A., Damy, T., Gillmore, J. D., Hazenberg, B. P., et al. (2022). Tissue biopsy for the diagnosis of amyloidosis: experience from some centres. *Amyloid* 29, 8–13. doi:10.1080/13506129.2021.1994386

Borsagli, F. G. M., Ciminelli, V. S., Ladeira, C. L., Haas, D. J., Lage, A. P., and Mansur, H. S. (2019). Multi-functional eco-friendly 3D scaffolds based on N-acyl thiolated chitosan for potential adsorption of methyl orange and antibacterial activity against *Pseudomonas aeruginosa*. *J. Environ. Chem. Eng.* 7, 103286. doi:10.1016/j.jece.2019.103286

Calzaferri, G., Gallagher, S. H., and Brühwiler, D. (2022). Multiple equilibria describe the complete adsorption isotherms of nonporous, microporous, and mesoporous adsorbents. *Microporous Mesoporous Mater.* 330, 111563. doi:10.1016/j.micromeso.2021.111563

Deloid, G. M., Yang, Z., Bazina, L., Kharaghani, D., Sadrieh, F., and Demokritou, P. (2024). Mechanisms of ingested polystyrene micro-nanoplastics (MNPs) uptake and translocation in an *in vitro* tri-culture small intestinal epithelium. *J. Hazard. Mater.* 473, 134706. doi:10.1016/j.jhazmat.2024.134706

Dendy, D., Lestari, W. W., Anshori, I., Surawijaya, A., Handayani, M., Wahyuningsih, S., et al. (2025). Enhanced indigo carmine adsorption using ethylenediamine-modified MIL-101 (Cr) materials. *Mater. Chem. Phys.* 334, 130465. doi:10.1016/j.matchemphys.2025.130465

Ding, A., He, Y., Chen, F.-F., and Yu, Y. (2024). Antibacterial activity of M-MOF nanomaterials (M= Fe, Co, Ni, Cu, and Zn): impact of metal centers. *ACS Appl. Nano Mater.* 7, 24571–24580. doi:10.1021/acsanm.4c04319

Farasati Far, B. (2024). "Antimicrobial properties of metal-organic frameworks," in *Logic for Metal– organic framework selection: MOFs for biomedical applications* (ACS Publications), 147–180. Available online at: https://pubs.acs.org/doi/abs/10.1021/bk-2024-1463.ch007

Feng, W., Feng, Y., He, Y., Chen, J., Wang, H., Luo, T., et al. (2022). Tuning the electronic communication of the Ru–O bond in ultrafine Ru nanoparticles to boost the alkaline electrocatalytic hydrogen production activity at large current density. *Inorg. Chem. Front.* 9, 4151–4159. doi:10.1039/d2qi00847e

Głowniak, S., Szczęśniak, B., Choma, J., and Jaroniec, M. (2021). Advances in microwave synthesis of nanoporous materials. *Adv. Mater.* 33, 2103477. doi:10.1002/adma.202103477

Ho, S. (2022). Low-cost adsorbents for the removal of phenol/phenolics, pesticides, and dyes from wastewater systems: a review. *Water* 14, 3203. doi:10.3390/w14203203

Holzwarth, U., and Gibson, N. (2011). The Scherrer equation versus the'Debye-Scherrer equation. *Nat. Nanotechnol.* 6, 534. doi:10.1038/nnano.2011.145

Hsu, C.-Y., Ali, E., Alamir, H. T. A., Jawad, M. A., Alsaadi, S. B., Karim, M. M., et al. (2024). Synthesis of new Ampicillin supported on Cr/Oxidized pectin supported on Ti bimetal–organic framework as an efficient antimicrobial and anticancer nanocomposite. *Inorg. Chem. Commun.* 165, 112566. doi:10.1016/j.inoche.2024.112566

Hu, Q., Lan, R., He, L., Liu, H., and Pei, X. (2023). A critical review of adsorption isotherm models for aqueous contaminants: curve characteristics, site energy distribution and common controversies. *J. Environ. Manag.* 329, 117104. doi:10.1016/j.jenvman.2022.117104

Hu, W., Ouyang, Q., Jiang, C., Huang, S., Alireza, N.-E., Guo, D., et al. (2024). Biomedical Metal–Organic framework materials on antimicrobial therapy: perspectives and challenges. *Mater. Today Chem.* 41, 102300. doi:10.1016/j.mtchem.2024.102300

Idris, D. S., Roy, A., Malik, A., Khan, A. A., Sharma, K., and Roy, A. (2024). Green synthesis of silver oxide-nickel oxide bimetallic nanoparticles using peels of citrus sinensis and their application. *J. Inorg. Organomet. Polym. Mater.* 35, 594–606. doi:10.1007/s10904-024-03316-9

Jin, J., Han, X., Fang, Y., Zhang, Z., Li, Y., Zhang, T., et al. (2022). Microenvironment engineering of Ru single-atom catalysts by regulating the cation vacancies in NiFe-layered double hydroxides. *Adv. Funct. Mater.* 32, 2109218. doi:10.1002/adfm.202109218

Kecskeméti, G., Tóth-Molnár, E., Janáky, T., and Szabó, Z. (2022). An extensive study of phenol red thread as a no*vel non-*invasive tear sampling technique for proteomics studies: comparison with two commonly used methods. *Int. J. Mol. Sci.* 23, 8647. doi:10.3390/ijms23158647

Khandan, F. M., Afzali, D., Sargazi, G., and Gordan, M. (2018). Novel uranyl-curcumin-MOF photocatalysts with highly performance photocatalytic activity toward the degradation of phenol red from aqueous solution: effective synthesis route, design and a controllable systematic study. *J. Mater. Sci. Mater. Electron.* 29, 18600–18613. doi:10.1007/s10854-018-9978-z

Lau, K. S., Chin, S. X., Khiew, P. S., Zakaria, S., Yin, M. L. J., Key, K. H. M., et al. (2022). Enhanced adsorption of anionic phenol red using cationic polyethylenimine-incorporated chitosan beads. *J. Porous Mater.* 29, 609–619. doi:10.1007/s10934-022-01198-1

Li, C., Wei, H., Hua, R., He, X., Lu, J., Chen, Q., et al. (2025). 3D Cu-BTC anchored on 2D MXene nanosheets using surface control approach for urea adsorption to achieve the regeneration of dialysate. *Sep. Purif. Technol.* 373, 133594. doi:10.1016/j.seppur.2025.133594

Li, R., Chen, T., and Pan, X. (2021). Metal–organic-framework-based materials for antimicrobial applications. *ACS nano* 15, 3808–3848. doi:10.1021/acsnano.0c09617

Liu, J., Shi, L., Wang, Y., Li, M., Zhou, C., Zhang, L., et al. (2022). Ruthenium-based metal-organic framework with reactive oxygen and nitrogen species scavenging activities for alleviating inflammation diseases. *Nano Today* 47, 101627. doi:10.1016/j.nantod.2022.101627

Moghaddam-Manesh, M., Darvishi, R., and Moshkriz, A. (2024). Innovative high-performance antimicrobial agent and dye adsorbent based on magnetic/copper nanoparticles. *J. Polym. Environ.* 32, 5231–5253. doi:10.1007/s10924-024-03289-3

Moghaddam-Manesh, M., Ghazanfari, D., Sheikhhosseini, E., and Akhgar, M. (2020). Synthesis of bioactive magnetic nanoparticles spiro [indoline-3, 4′-[1, 3] dithiine]@ Ni (NO3) 2 supported on Fe3O4@ SiO2@ CPS as reusable nanocatalyst for the synthesis of functionalized 3, 4-dihydro-2H-pyran. *Appl. Organomet. Chem.* 34, e5543. doi:10.1002/aoc.5543

Mousavi, S. M., Meraji, S. H., Sanati, A. M., and Ramavandi, B. (2023). Phenol red dye removal from wastewater using TiO2-FSM-16 and Ni-FSM-16 photocatalysts. *Heliyon* 9, e14488. doi:10.1016/j.heliyon.2023.e14488

Moxley, R. A. (2022). *Enterobacteriaceae: Shigella*. Veterinary Microbiology, 100–107. Available online at: https://onlinelibrary.wiley.com/doi/abs/10.1002/9781119650836.ch9

Nakhjiri, A. T., Sanaeepur, H., Amooghin, A. E., and Shirazi, M. M. A. (2022). Recovery of precious metals from industrial wastewater towards resource recovery and environmental sustainability: a critical review. *Desalination* 527, 115510. doi:10.1016/j.desal.2021.115510

Naseer, M. N., Jaafar, J., Junoh, H., Zaidi, A. A., Kumar, M., Alqahtany, A., et al. (2022). Metal-organic frameworks for wastewater decontamination: discovering intellectual structure and research trends. *Materials* 15, 5053. doi:10.3390/ma15145053

Nasiri, S., Rabiei, M., Palevicius, A., Janusas, G., Vilkauskas, A., Nutalapati, V., et al. (2023). Modified Scherrer equation to calculate crystal size by XRD with high accuracy, examples Fe2O3, TiO2 and V2O5. *Nano Trends* 3, 100015. doi:10.1016/j.nwnano.2023.100015

Olusegun, O. A., and Martincigh, B. S. (2021). Allergic contact dermatitis: a significant environmental and occupational skin disease. *Int. J. Dermatology* 60, 1082–1091. doi:10.1111/ijd.15502

Pang, B., Ma, Y., Tian, Z., Liu, J., Wu, S., Teng, D., et al. (2021). Solvents-dependent selective fabrication of face-centered cubic and hexagonal close-packed structured ruthenium nanoparticles during liquid-phase laser ablation. *J. Colloid Interface Sci.* 585, 452–458. doi:10.1016/j.jcis.2020.10.026

Peng, S., Ma, X., Tian, J., Du, C., Yang, L., Meng, E., et al. (2024). One-pot etching pyrolysis to defect-rich carbon nanosheets to construct multiheteroatom-coordinated iron sites for efficient oxygen reduction. *Small* 20, 2310637. doi:10.1002/smll.202310637

Perez Ortiz, A., Hahn, C., Schaible, T., Rafat, N., and Lange, B. (2021). Severe pneumonia in neonates associated with legionella pneumophila: case report and review of the literature. *Pathogens* 10, 1031. doi:10.3390/pathogens10081031

Pessoa, J. C., and Correia, I. (2021). Misinterpretations in evaluating interactions of vanadium complexes with proteins and other biological targets. *Inorganics* 9, 17. doi:10.3390/inorganics9020017

Poon, P.-C., Wang, Y., Li, W., Suen, D.W.-S., Lam, W. W. Y., Yap, D. Z. J., et al. (2022). Synergistic effect of Co catalysts with atomically dispersed CoN_x active sites on ammonia borane hydrolysis for hydrogen generation. *J. Mater. Chem. A* 10, 5580–5592. doi:10.1039/d1ta09750d

Pourmadadi, M., Ostovar, S., Eshaghi, M. M., Rajabzadeh-Khosroshahi, M., Safakhah, S., Ghotekar, S., et al. (2023). Nanoscale metallic-organic frameworks as an advanced tool for medical applications: challenges and recent progress. *Appl. Organomet. Chem.* 37, e6982. doi:10.1002/aoc.6982

Qin, G., Zou, K., He, F., Shao, J., Zuo, B., Liu, J., et al. (2023). Simultaneous determination of volatile phenol, cyanide, anionic surfactant, and ammonia nitrogen in drinking water by a continuous flow analyzer. *Sci. Rep.* 13, 1829. doi:10.1038/s41598-023-28776-w

Qiu, B., Shao, Q., Shi, J., Yang, C., and Chu, H. (2022). Application of biochar for the adsorption of organic pollutants from wastewater: modification strategies, mechanisms and challenges. *Sep. Purif. Technol.* 300, 121925. doi:10.1016/j.seppur.2022.121925

Raffay, R., Husin, N., and Omar, A. F. (2022). Spectrophotometry and colorimetry profiling of pure phenol red and cell culture medium on pH variation. *Color. Technol.* 138, 640–659. doi:10.1111/cote.12626

Rajendran, H. K., Deen, M. A., Ray, J. P., Singh, A., and Narayanasamy, S. (2024). Harnessing the chemical functionality of metal–organic frameworks toward removal of aqueous pollutants. *Langmuir* 40, 3963–3983. doi:10.1021/acs.langmuir.3c02668

Roy, S., Bhattacharjee, B., Mazumder, P. B., Bhattacharjee, M., Dhar, D., and Bhattacharjee, A. (2024). Molecular characterization of enteropathogenic *Escherichia coli* isolated from patients with gastroenteritis in a tertiary referral hospital of northeast India. *Indian J. Med. Microbiol.* 47, 100535. doi:10.1016/j.ijmmb.2024.100535

Sharafudheen, S. B., Vijayakumar, C., Anjana, P., Bindhu, M., Alharbi, N. S., Khaled, J. M., et al. (2024). Biogenically synthesized porous TiO2 nanostructures for advanced anti-bacterial, electrochemical, and photocatalytic applications. *J. Environ. Manag.* 366, 121728. doi:10.1016/j.jenvman.2024.121728

Siddique, N., Din, M. I., Khalid, R., and Hussain, Z. (2024). A comprehensive review on the photocatalysis of Congo red dye for wastewater treatment. *Rev. Chem. Eng.* 40, 481–510. doi:10.1515/revce-2022-0076

Singh, A., and Barman, P. (2021). Recent advances in Schiff base ruthenium metal complexes: synthesis and applications. *Top. Curr. Chem.* 379, 29–71. doi:10.1007/s41061-021-00342-w

Singh, S., Ahmed, A. I., Almansoori, S., Alameri, S., Adlan, A., Odivilas, G., et al. (2024). A narrative review of wastewater surveillance: pathogens of concern, applications, detection methods, and challenges. *Front. Public Health* 12, 1445961. doi:10.3389/fpubh.2024.1445961

Skoczynska, A., Lewinski, A., Pokora, M., Paneth, P., and Budzisz, E. (2023). An overview of the potential medicinal and pharmaceutical properties of Ru (II)/(III) complexes. *Int. J. Mol. Sci.* 24, 9512. doi:10.3390/ijms24119512

Song, C., and Qin, J. (2022). High-performance fabricated nano-adsorbents as emerging approach for removal of mycotoxins: a review. *Int. J. Food Sci. and Technol.* 57, 5781–5789. doi:10.1111/ijfs.15953

Southam, H. M., Butler, J. A., Chapman, J. A., and Poole, R. K. (2017). The microbiology of ruthenium complexes. *Adv. Microb. physiology* 71, 1–96. doi:10.1016/bs.ampbs.2017.03.001

Steinegger, A., Wolfbeis, O. S., and Borisov, S. M. (2020). Optical sensing and imaging of pH values: spectroscopies, materials, and applications. *Chem. Rev.* 120, 12357–12489. doi:10.1021/acs.chemrev.0c00451

Tan, Q., Chen, Z., Liu, L., and Huang, X. (2023). Functionalized rhodium nanoparticles as antimicrobial agents for treatment of drug-resistant skin and soft tissue infections. *Adv. Healthc. Mater.* 12, 2203200. doi:10.1002/adhm.202203200

Tee, S. Y., Lee, C. J. J., Dinachali, S. S., Lai, S. C., Williams, E. L., Luo, H.-K., et al. (2015). Amorphous ruthenium nanoparticles for enhanced electrochemical water splitting. *Nanotechnology* 26, 415401. doi:10.1088/0957-4484/26/41/415401

Wang, D., Ying, Y., Cai, L., Cheng, H., Giannakis, S., Moussavi, G., et al. (2025). Acid-engineered UiO-66 (Ce): from the limitations of concealed MOF sites to catalytic excellence for rapid atrazine degradation. *Chem. Eng. J.* 516, 163890. doi:10.1016/j.cej.2025.163890

Wang, K., Zhou, J., Sun, M., Lin, F., Huang, B., Lv, F., et al. (2023). Cu-Doped heterointerfaced Ru/RuSe2 nanosheets with optimized H and H2O adsorption boost hydrogen evolution catalysis. *Adv. Mater.* 35, 2300980. doi:10.1002/adma.202300980

Weiskirchen, S., Schröder, S. K., Buhl, E. M., and Weiskirchen, R. (2023). A beginner's guide to cell culture: practical advice for preventing needless problems. *Cells* 12, 682. doi:10.3390/cells12050682

Wu, Z., Ye, X., Liu, H., Zhang, H., Liu, Z., Guo, M., et al. (2020). Interactions between adsorbents and adsorbates in aqueous solutions. *Pure Appl. Chem.* 92, 1655–1662. doi:10.1515/pac-2019-1110

Yao, T., Zeng, X., Tao, X., and Xu, H. (2024). Recent progress of MOF-based antibacterial hydrogels. *Chem. Eng. J.* 487, 150641. doi:10.1016/j.cej.2024.150641

Yesil, H., Molaey, R., Calli, B., and Tugtas, A. E. (2021). Extent of bioleaching and bioavailability reduction of potentially toxic heavy metals from sewage sludge through pH-controlled fermentation. *Water Res.* 201, 117303. doi:10.1016/j.watres.2021.117303

Zhang, J., Xie, M., Zhao, H., Zhang, L.-R., Wei, G., and Zhao, G. (2021). Preferential and efficient degradation of phenolic pollutants with cooperative hydrogen-bond interactions in photocatalytic process. *Chemosphere* 269, 129404. doi:10.1016/j.chemosphere.2020.129404

Zhang, X., Zhang, K., Shi, Y., Xiang, H., Yang, W., and Zhao, F. (2024). Surface engineering of multifunctional nanostructured adsorbents for enhanced wastewater treatment: a review. *Sci. Total Environ.* 920, 170951. doi:10.1016/j.scitotenv.2024.170951

Zhou, X., Zhu, Q., Zheng, A., Xue, B., Wang, Q., Chin, L., et al. (2024). *De novo* design of covalent bonding peptides for target protein. *hLife* 2, 641–652. doi:10.1016/j.hlife.2024.07.007

Zouganeli, V., Kourek, C., Bistola, V., Mademli, M., Grigoropoulos, I., Thomas, K., et al. (2024). Campylobacter jejuni-related myocarditis: a case report and review of the literature. *J. Clin. Med.* 13, 7551. doi:10.3390/jcm13247551